Design Methodology for Barrier-Based Two Phase Flow Distributor

Ma'moun Al-Rawashdeh and Xander Nijhuis
Dept. of Chemical Engineering and Chemistry, Laboratory of Chemical Reactor Engineering, Eindhoven University of Technology, 5600 MB Eindhoven, The Netherlands

Evgeny V. Rebrov
Reactor and Process Engineering, School of Chemistry and Chemical Engineering, Queen's University Belfast, BT9 5AG Belfast, UK

Volker Hessel and Jaap C. Schouten
Dept. of Chemical Engineering and Chemistry, Laboratory of Chemical Reactor Engineering, Eindhoven University of Technology, 5600 MB Eindhoven, The Netherlands

DOI 10.1002/aic.13750
Published online February 17, 2012 in Wiley Online Library (wileyonlinelibrary.com).

The barrier-based distributor is a multiphase flow distributor for a multichannel microreactor which assures flow uniformity and prevents channeling between the two phases. For N *number of reaction channels, the barrier-based distributor consists of a gas manifold, a liquid manifold,* N *barrier channels for the gas,* N *barrier channels for the liquid, and* N *mixers for mixing the phases before the reaction channels. The flow distribution is studied numerically using a method based on the hydraulic resistive networks (RN). The single phase hydraulic RN model (Commenge et al., 2002;48:345–358) is extended for two phases gas-liquid Taylor flow. For* Re_{GL} *<30, the accuracy for the model was above 90%. The developed-model was used to study the effects of fabrication tolerance and barrier channel dimensions. A design methodology has been proposed as an algorithm to determine the required hydraulic resistance in the barrier channels and their dimensions. This methodology is demonstrated using a numerical example.* © 2012 American Institute of Chemical Engineers *AIChE J,* 58: 3482–3493, 2012

Keywords: flow distribution, microreactor, numbering-up, fabrication tolerance, hydraulic resistance network

Introduction

Reactions in micro and millimeter scale channels can benefit from enhanced mass and heat transfer characteristics. This is why micrometer and millimeter channels are excellent for Process Intensification and for operation in the concept of Novel Process Window.[1–5] The throughput of a single micrometer or millimeter scale reaction channel is often not more than few milliliter per minute, which can be increased via two possible routes. The first scaling route is by ''smart'' scale-up, increasing the internal channel cross section, while keeping the enhanced mass and heat transfer characteristics. Smart scale-up has been successfully demonstrated for single phase processes. Lonza Company has presented a smart increase of channel diameter, with even changing microreactor types, from laboratory over pilot to production-scale.[6] Additionally, operation in the Novel Process Windows allows a rate acceleration of liquid-phase reactions so that even with keeping a channel diameter small, a large productivity in one channel can be realized.

For multiphase flows, the situation is different. Increasing the channel diameter slightly can change the flow patterns,[7] which provide the characteristic of the process and the key to its process intensification. For gas–liquid flows, difficulties might arise through the different impacts of temperature and pressure on gas and liquid; for example, a gas will be compressed under pressure which will change the flow pattern notably.

The second scaling route is ''numbering-up'', that is, placing channels in parallel. The key for successful numbering-up is equalizing the flow distribution over the channels. The scaling route for numbering-up is shown in Figure 1. Distribution of multiphase flow takes place only in parallel channels in a plate (ii) where mixing of the two phases occurs. A single phase flow feeding system is required at the subsequent levels of parallel plates (iii) and parallel modules (iv). This simplifies the handling of the connectors in a confined system considerably. In fuel processing, catalytic gas-phase microreactors with thousands of parallel microchannels are state of the art and flow distributors are available, give sufficient equipartition, and are part of patent literature.[8–10] In

Correspondence concerning this article should be addressed to J.C. Schouten at J.C.Schouten@tue.nl.

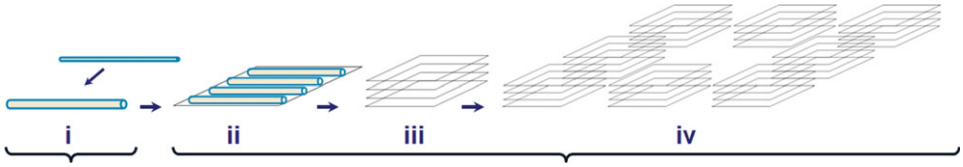

Figure 1. Scaling route for microchannel reactor to larger scale throughput.

(i) Scale-up of a single channel, (ii) parallel channels in plate, (iii) parallel plates in a modular, (iv) parallel modular's in one operation unit. From (ii) to (iv) only numbering-up is used to increase the throughput. [Color figure can be viewed in the online issue, which is available at wileyonlinelibrary.com.]

liquid-phase processing, numbering-up has been demonstrated as well, although often at a much lower number of channels operated in parallel or even as external numbering-up with a very few devices.[11]

Flow distribution for multiphase flow in microchannels, and in particular for gas–liquid flow, is not as straightforward as for single phase flow. Improper flow distribution does not only change the flow uniformity, but it also can result in a deformation of the flow pattern or in gas–liquid channeling, some channels filled only with liquid while others are filled with gas.

The barrier-based distributor, which is shown in Figure 2, is a multiphase flow distributor which prevents gas–liquid channeling, operates in the whole range of gas and liquid flow patterns, and significantly reduces flow nonuniformity.[12–14] It consists of hydraulic flow resistances between the single phase flow distributors and the parallel channels to minimize the interaction between these parts. The hydraulic flow resistance of the barrier channels can be quantified using Eq. 1 as $\Delta\tilde{P}_B$. It is the average pressure drop over the barrier channels $\overline{\Delta P_B}$ divided by the average pressure drop over the corresponding mixers and microchannels $\overline{\Delta P_C}$. As $\Delta\tilde{P}_B$ is a ratio of pressure drops, it is dimensionless

$$\Delta\tilde{P}_B = \frac{\overline{\Delta P_B}}{\overline{\Delta P_C}} \quad (1)$$

Mixing two phases in a microchannel can result in different flow patterns; Taylor flow [7,15] is industrially most attractive due to its well-defined shape, reduced axial dispersion almost approaching ideal plug flow,[16] and improved mass and heat transfer.[17–20] In a setup of four channels operated in the Taylor flow regime, we experimentally studied the influence of $\Delta\tilde{P}_B$ on the flow nonuniformity.[21] The most important findings were that a flow nonuniformity less than 10% is reached when $\Delta\tilde{P}_B$ is in the range of 4–25, and that the flow nonuniformity is proportional to four times the variation in the inner diameter of the barrier channels. By comparing our finding to that of de Mas et al.[13] who were one of the first to introduce the barrier-channel concept in microchannels, the dimensions of the gas and liquid barrier channels were chosen to create a $\Delta\tilde{P}_B$ of 50 and 25, respectively. This value for $\Delta\tilde{P}_B$ is already beyond the optimal which should be between 4 and 25. Larger than this optimal limit, the flow distribution is mainly controlled by the pressure drop in the barrier channels. This was confirmed by de Mas et al.[13] They mentioned that the flow nonuniformity scales with the pressure drop in the barrier channels that scales with the diameter of the channels to the power four (d^4).

The design approach of de Mas et al.[13] can be regarded as the safe approach, because they were not concerned about the energy dissipation – the pressure drop of the distributor is beyond the optimal range. Their design approach can be summarized as: first, the pressure drop over the reaction channels is measured; second, the dimensions for the barrier channels are chosen to provide a $\Delta\tilde{P}_B$ larger than 25; last, the flow nonuniformity is linearly scaled with the variation in the channel diameter of the barrier channels with a factor of 4.

In case, an optimal distributor design is needed (optimal refers to when $\Delta\tilde{P}_B$ is between 4 and 25), the approach by de Mas et al.[13] is not valid any more. The cross talk between the distributor and the downstream parts increases. An improved insight in the relation of the fabrication tolerance, not only in the barrier-channels but also in all parts of the device are crucial to reach a desired target flow uniformity.

Our previous work[21] quantified the flow nonuniformity as a function of $\Delta\tilde{P}_B$ and the variation in the inner diameter for barrier, mixer, and reaction channels. However, for a target flow nonuniformity, it did not provide steps on how to determine the exact barrier channels dimensions, fabrication tolerance and how to extend the work to other flow regimes. Here, we aim at determining these targets by developing a design methodology for the barrier-based distributor using a two phase resistive network (RN) model. In the next section, this model is introduced followed by the conceptual idea of the design methodology. After the methods, results and discussion, we conclude by providing the step-by-step design methodology. A numerical example is provided to illustrate the design.

2-Phase RN model

The design principle for flow distributors relies on controlling the hydraulic flow resistance, described by the pressure

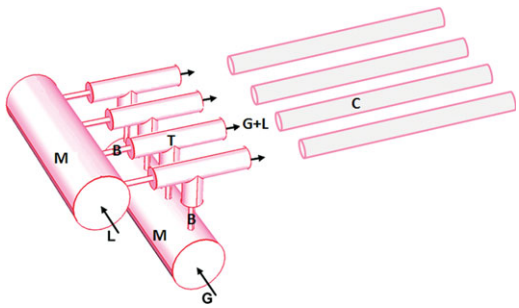

Figure 2. Schematic representation of barrier-based gas–liquid flow distributor for four parallel microchannels.

Symbols used are: (G) gas, (L) liquid, (M) manifold, (B) barrier channel, (T) T-mixer, and (C) reaction channel. [Color figure can be viewed in the online issue, which is available at wileyonlinelibrary.com.]

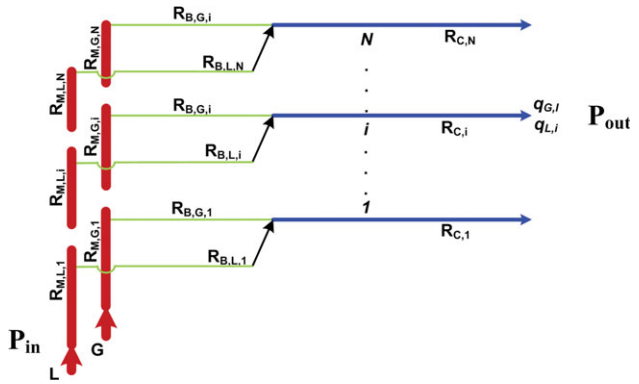

Figure 3. Schematic view for simplified gas-liquid flow resistive network.

***R* is the hydraulic flow resistance defined in Eq. 2. The index used for each parameter is M manifold, B barrier, C reaction channel, *q* flow rate, G gas, L liquid, *i* is a variable for the number of channels *N*. [Color figure can be viewed in the online issue, which is available at wileyonlinelibrary.com.]**

drop in each channel. In micro-fluidic devices, the RN model is often used to design and understand the influence of these resistances.[22,23] Most RN models are developed for single phase flow and are only valid at relatively low Reynolds number in the laminar regime. Here, the RN model is extended to account for multiphase flow, the 2-phase resistive network (2-*PRN*) model. A simplified example for gas-liquid resistive flow network is shown in Figure 3. Gas and liquid are distributed to parallel channels using a consecutive ladder manifold. The gas flow passes through its own barrier channels and the liquid flow passes through its own barrier channels. The gas and liquid flows are mixed in a T-mixer and the gas–liquid flow passes through the reaction channels. The pressure drop in each segment line can be written according to Eq. 2, as the multiplication of the hydraulic resistance (R) by the flow rate (q). An explanation of the hydraulic resistances and their types are given in details in the Appendix

$$\Delta P = R\, q \tag{2}$$

Regardless of the flow path, the pressure drop from *in* to *out* is equal to $P_{in} - P_{out}$. The pressure of the gas and liquid manifold are equal, because gas–liquid channeling is prevented when $P_{in,G} = P_{in,L}$.[21] The pressure drop for each flow path can be written as a summation of the pressure drop in series and equals to $P_{in} - P_{out}$. The pressure drop for flow path of channel number i can be written as

$$\begin{aligned} P_{in} - P_{out} &= \Delta P_{M,L,i} + \Delta P_{B,L,i} + \Delta P_{C,i} \\ &= \Delta P_{M,G,i} + \Delta P_{B,G,i} + \Delta P_{C,i} \end{aligned} \tag{3}$$

$\Delta P_{M,L,i}$ is the pressure drop in the liquid manifold for the region between channels $i-1$ and i. $\Delta P_{B,L,i}$ is the pressure drop for the liquid flow in barrier channel number i. $\Delta P_{C,i}$ is the pressure drop of the gas–liquid flow in mixer and reaction channel number i. Equation 3 can be rewritten in the hydraulic resistance form to Eqs. 4 and 5 for the liquid and gas phase, respectively. By simultaneously solving the pressure drop equations and the mass balances for both gas and liquid and for all parallel channels, the flow distribution can be computed. A detailed analysis of how to arrange and solve these equations is provided in the Appendix

$$\begin{aligned} P_{in} - P_{out} &= R_{M,L,i}\,(q_{M,L,i}) + R_{B,L,i}\,(q_{B,L,i}) \\ &\quad + R_{C,i}\,(q_{C,L,i} + q_{C,G,i}) \end{aligned} \tag{4}$$

$$\begin{aligned} P_{in} - P_{out} &= R_{M,G,i}\,(q_{M,G,i}) + R_{B,L,i}\,(q_{B,G,i}) + R_{C,i}\,(q_{C,L,i} \\ &\quad + q_{C,G,i}) \end{aligned} \tag{5}$$

Design methodology

The 2-PRN model provides the basis of the design methodology. The conceptual idea of the design methodology is to analytically decouple the target flow nonuniformity $\sigma(\tilde{q})$ into cumulative contributions of three flow nonuniformity factors: manifold $\sigma(\tilde{q}_M)$, barrier $\sigma(\tilde{q}_B)$, and mixers and reaction channels $\sigma(\tilde{q}_C)$ as shown in Eq. 6. Each flow nonuniformity factor represents part of the hydraulic resistances that compose the total two phase RN. Before proceeding to explain these flow nonuniformity factors, the following definitions are explained

$$\sigma(\tilde{q}) = \sqrt{\sigma^2(\tilde{q}_M) + \sigma^2(\tilde{q}_B) + \sigma^2(\tilde{q}_C)} \tag{6}$$

$\sigma(\tilde{q})$ is the target flow nonuniformity quantified as the relative standard deviations σ according to Eq. 7; $\tilde{q}_i$ is the flow rate per channel normalized by $\bar{q}$ as defined in Eq. 8; $\bar{q}$ is the average flow rate per channel (Eq. 9); q_i is the flow rate per channel; N is the number of channels

$$\sigma(\tilde{q}) = \frac{1}{\bar{q}}\sqrt{\frac{\Sigma_i(\tilde{q}_i - \bar{q})^2}{N-1}}\,100\% \tag{7}$$

$$\tilde{q}_i = \frac{q_i}{\bar{q}} \tag{8}$$

$$\bar{q} = \frac{\sum_{i=1}^{i=N} q_i}{N} \tag{9}$$

The three flow nonuniformity factors are:

The manifold flow nonuniformity factor, $\sigma(\tilde{q}_M)$. This factor quantifies the flow nonuniformity due to the influence of manifold type and dimensions. It is computed for single phase flow only. It quantifies the influence of the the manifold on the flow distribution without the influence of (1) second phase, (2) variation in the hydraulic resistance due to the fabrication tolerance, and (3) without the use of the barrier channels. This is shown in a simplified manner in Figure 4a. The resulted flow per channel is q_M. By normalizing q_M according to Eq. 10, the relative standard deviation of $\tilde{q}_M$ can be computed which is the manifold flow nonuniformity factor $\sigma(\tilde{q}_M)$.

$$\tilde{q}_{M,i} = \frac{q_{M,i}}{\bar{q}}. \tag{10}$$

The following conditions have been used to evaluate $\sigma(\tilde{q}_M)$:

- Fixed physical properties.
- Uniform manifold cross section area, $R_{M,i}$ = constant.
- The hydraulic resistances of the barrier channels are negligible, $R_{B,i} = 0$.

Table 1. Dimensions of Channels in (mm) Used in the Simulation Study of Figure 6

	H	*W*	*L*	d
Manifold	4	40	4	–
Reaction	1	1	2000	
Slit liquid barrier	0.05–1.35*	0.6	150	–
Slit gas barrier	0.01–0.3*	0.45	150	–
Circular liquid barrier	–	–	150	0.05–0.5*
Circular gas barrier	–	–	150	0.05–0.5*

The * refers to channels where fabrication tolerance are added according to Eq. 14. For each set of channel dimensions, simulation of the fabrication tolerance is repeated 1000 times. N is kept fixed to 40, Re_{GL} to 85 and $\frac{q_G}{q_L}$ to 1.

• No variation in the channel diameters due to the fabrication tolerance: $R_{B,i}$ = constant, $R_{C,i}$ = constant.

The barrier flow nonuniformity factor, $\sigma(\tilde{q}_B)$. This factor quantifies the flow nonuniformity due to the variation in the inner diameter of the barrier channels. It is computed for single phase flow. By extending the scheme shown in Figure 3a to include the barrier channels with variations in their inner diameters, $\sigma(\tilde{q_B})$ are computed. So, $\sigma(\tilde{q_B})$ quantifies how much the flow distribution changes as a result of introducing the barrier channels. It is shown in a simplified manner in Figure 4b. The resulting flow per channel for this step is q_B. By normalizing q_B according to Eq. 11, the relative standard deviation of $\tilde{q_B}$ can be computed which is the barrier factor $\sigma(\tilde{q_B})$

$$\tilde{q}_{B,i} = \frac{q_{B,i}}{q_{M,i}} \tag{11}$$

The following conditions have been used to evaluate $\sigma(\tilde{q_B})$:

• Fixed physical properties.

• Uniform manifold cross section area, $R_{M,i}$ = constant.

• The hydraulic resistances for the barrier channels are taken into account, $R_{B,i} > R_{C,i}$.

• The variation in the barrier channel diameters due to the fabrication tolerance are considered, $R_{B,i} \neq$ constant.

• The variations in the mixer and reaction channel diameters due to the fabrication tolerance are not taken into account, $R_{C,i}$ = constant.

The mixers and reaction channels flow nonuniformity factor, $\sigma(\tilde{q}_C)$. This factor quantifies the influence of variation in the mixers and reaction channels diameters and the influence of the second phase on the flow nonuniformity. It is computed for two-phases flow and is shown in a simplified manner in Figure 4c. By extending the scheme shown in Figure 4b to take into account: (1) the second phase, (2) mixers, and (3) variations in the mixers and reaction channels diameters due to the fabrication tolerance, $\sigma(\tilde{q_C})$ can be calculated. So, $\sigma(\tilde{q_C})$ quantifies how much the flow distribution is affected due to these additions. The flow per channel for this step is q_C. By normalizing q_C according to Eq. 12, the relative standard deviation of $\tilde{q_C}$ can be computed which is the mixer and reaction channels flow nonuniformity factor, $\sigma(\tilde{q_C})$

$$\tilde{q}_{C,i} = \frac{q_i}{q_{B,i}} \tag{12}$$

The following conditions have been used to evaluate $\sigma(\tilde{q_C})$:

• Fixed physical properties.

• Uniform manifold cross section area, $R_{M,i}$ = constant.

• The hydraulic resistances for the barrier channels are taken into account, $R_{B,i} > R_{C,i}$.

• The variation in the barrier channels diameters due to the fabrication tolerance are considered, $R_{B,i} \neq$ constant.

• The variations in the mixer and reaction channel diameters due to the fabrication tolerance are considered, $R_{C,i} \neq$ constant.

The product of $\tilde{q_M}$, $\tilde{q_B}$, and $\tilde{q_C}$ yields the actual flow per channel $\tilde{q}$ (Eq. 13)

$$\tilde{q}_i = \tilde{q}_{M,i}\, \tilde{q}_{B,i}\, \tilde{q}_{C,i} \tag{13}$$

Correlations for the three flow nonuniformity factors σ ($\tilde{q_M}$), $\sigma(\tilde{q_B})$, and $\sigma(\tilde{q_C})$ are obtained using the 2-PRN model. These correlations are derived for a range of conditions as shown in Tables 1–3. When the channel geometry is rectangular, H, W, and L are the depth, width, and length of the channel. When the channel geometry is circular, d and L are the diameter and length of the channel, respectively. H_{mixer} and $W_{mixer,G,in}$ are the depth of the channels in a T-mixers and width of inlet gas channel in a T-mixer, respectively.

The simulation study is performed for gas–liquid flow operating in the Taylor flow regime. Pressure drop of Taylor flow was calculated by the model proposed by Warnier et al.[24] The slug and bubble lengths in a T-mixer were estimated by the model proposed by van Steijn et al.[25] For investigating the effect of fabrication tolerance, a random variation (δ_f) was added to the inner channel diameters using Eq. 14 following a normalized random distribution. In the barrier channels, the influence of fabrication tolerance was studied for two types of channel cross sectional geometry: circular and slit - rectangular channel with a width over depth larger than 2 as shown in Table 1.

$$d_i = \overline{d} \pm \delta_f \tag{14}$$

Results and Discussion

Influence of the manifold flow nonuniformity factor, $\sigma(\tilde{q}_M)$

At different hydraulic flow resistance ratios R_C/R_M and numbers of parallel channels N, the calculated manifold flow nonuniformity factor $\sigma(\tilde{q_M})$ is shown in Figure 5. As R_C/R_M

Table 2. Dimensions of Channels in (mm) Used in the Simulation Study of Figure 7

	H	*W*	*L*	H_{mixer}	$W_{mixer,G,in}$
Manifold	4	40	4	–	–
Liquid barrier	0.045–0.225*	0.6	150	–	–
Gas barrier	0.01–0.05*	0.45	150	–	–
Mixer	–	–	–	1*	1*
Reaction	0.1–3*	0.1–3*	2000	–	–

The * refers to channels where fabrication tolerance are added according to Eq. 14. For each set of channel dimensions, simulation of the fabrication tolerance is repeated 1000 times. N is changed from 10 to 200, and Re_{GL} from 1 to 250 and $\frac{q_G}{q_L}$ is kept fix to 1.

Table 3. Dimensions of Channels in (mm) Used in the Simulation Study of Figure 10

	H	*W*	*L*	H_{mixer}	$W_{mixer,G,in}$
Manifold	4	40	4	–	–
Liquid barrier	0.05–1.35*	0.06–1.8	150	–	–
Gas barrier	0.01–0.3*	0.05–1.35	150	–	–
Mixer	–	–	–	0.1–3*	0.1–3*
Reaction	1*	1*	2000	–	–

The * refers to channels where fabrication tolerance are added according to Eq. 14. For each set of channel dimensions, simulation of the fabrication tolerance is repeated 1000 times. N is kept fixed to 40, Re_{GL} to 85 and $\frac{q_G}{q_L}$ to 1.

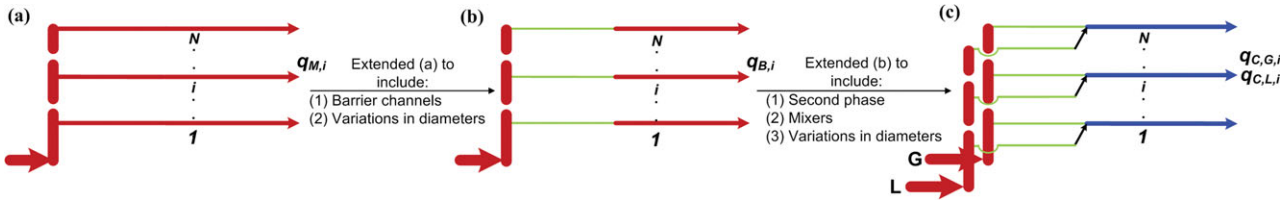

Figure 4. Schematic view of how the simplified two-phases RN shown in Figure 3 is decoupled into three steps.

Step (a) shows the manifold and reaction channels; step (b) extends step (a) to include the barrier channels; step (c) extends step (b) by including mixers and second phase. [Color figure can be viewed in the online issue, which is available at wileyonlinelibrary.com.]

increases or as N decreases, the manifold flow nonuniformity factor $\sigma(\tilde{q}_M)$ decreases. This behavior is similar to that shown by Amador et al.[22] To provide a better physical interpretation for Figure 5, a dimensionless analysis for two channels in parallel (arranged consecutively) is derived for the case shown in Figure 4a. Using Eq. 2 and assuming that the overall pressure drop is constant, the flow rate q depends just on the overall equivalent hydraulic resistance R_{eq}, shown as $q = \frac{\Delta P}{R_{eq}}$. Using the equivalent resistance concept in an electrical network, the equivalent resistance R_{eq} for two parallel channels is given by Eq. 15. This equation explains the flow nonuniformity trend observed in Figure 5. For the case when R_C is much larger than R_M, the equivalent resistance equals to $\frac{1}{R_{eq}} = \frac{2}{R_C}$. The 2 here refers to the number of parallel channels, which explains the dependency on the number of parallel channels.

$$\frac{1}{R_{eq}} = \frac{(R_C)_1 + (R_C + R_M)_2}{(R_C)_1 (R_C + R_M)_2} \tag{15}$$

$$\sigma(\tilde{q}_M) = 14.71\, N^{1.90} \left(\frac{R_C}{R_M}\right)^{-0.96} \tag{16}$$

The aim in this section is to extract an empirical correlation for $\sigma(\tilde{q}_M)$ to demonstrate the design methodology. For this purpose, the result in Figure 5 were fitted, which resulted in Eq. 16. The fitted values are for a manifold with a uniform and constant manifold cross sectional area. For other types of manifolds,[26] the fitted values might not be appropriate. The 95% confidence intervals of the fitting parameters are 14.47–15.06, 1.89–1.95, and −.98 to −0.95 as shown in Eq. 16, respectively.

Influence of the barrier channels flow nonuniformity factor, $\sigma(\tilde{q}_B)$

For different hydraulic resistance of the barrier channels $\Delta\tilde{P}_B$, the barrier flow non uniformity factor $\sigma(\tilde{q}_B)$ is studied as a function of the variation in the inner diameter of the barrier channels $\sigma(d_B)$. By dividing the flow nonuniformity over $\sigma(d_B)$, the influence of $\Delta\tilde{P}_B$ is shown in Figure 6. The result for the circular and slit are compared at the same value of hydraulic resistance. When a large hydraulic resistance in the barrier channels is used, the relation between $\sigma(\tilde{q}_B)$, $\sigma(d_B)$ and $\Delta\tilde{P}_B$ starts approaching a constant values of 4 and 3 for the circular and slit channel geometry, respectively. This trend can be explained by performing dimensionless analysis similar to the one made in the previous section but for the case shown in Figure 4b. The equivalent resistance for two channels in parallel are derived, as shown in 17. The flow rate q depends linearly on $\frac{1}{R_{eq}}$

$$\frac{1}{R_{eq}} = \frac{(R_B + R_C)_1 + ((R_B + R_C)_2 + (R_M)_2)}{(R_B + R_C)_1((R_B + R_C)_2 + (R_M)_2)}. \tag{17}$$

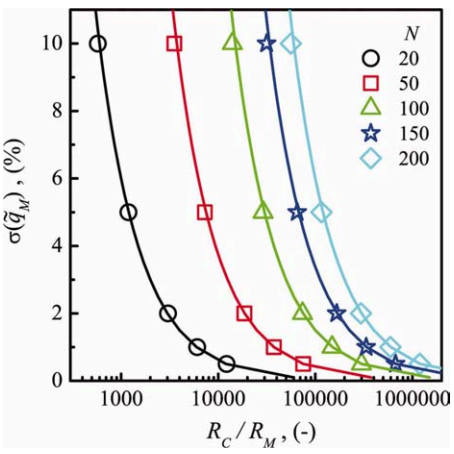

Figure 5. The influence of the hydraulic flow resistance ratio R_C/R_M on the manifold flow nonuniformity factor, $\sigma(\tilde{q}_M)$, as a function of parallel channels N.

This is obtained using the 2-PRN model for a manifold with a uniform and constant cross sectional area shown in Figure 4a. [Color figure can be viewed in the online issue, which is available at wileyonlinelibrary.com.]

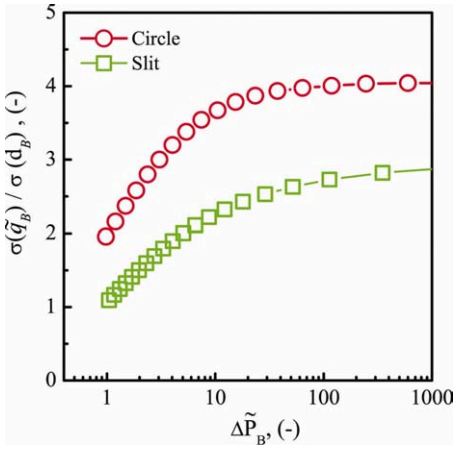

Figure 6. The barrier channels flow nonuniformity $\sigma(\tilde{q}_B)$ divided over the variation in the inner diameter of the barrier channels, $\sigma(d_B)$ at different value of $\Delta\tilde{P}_B$.

This study is done for circular and slit barrier channels geometries for the system shown in Figure 4b. The result for both geometry are computed at the same value of hydraulic resistance. [Color figure can be viewed in the online issue, which is available at wileyonlinelibrary.com.]

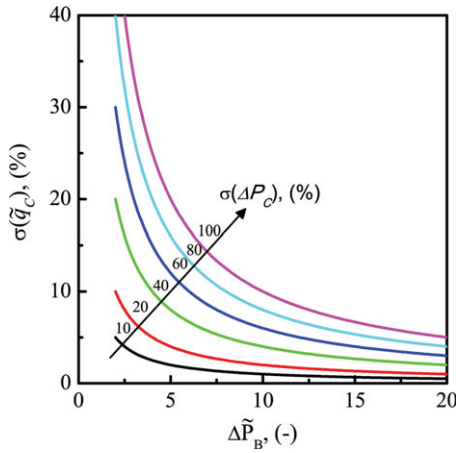

Figure 7. The influence of $\sigma(\Delta P_C)$ on $\sigma(\tilde{q}_C)$ at different values of $\Delta\tilde{P}_B$.

The study is performed for the system shown in Figure 3c. [Color figure can be viewed in the online issue, which is available at wileyonlinelibrary.com.]

When R_B is much larger than R_M and R_C (large hydraulic resistance in the barrier channels), then the equivalent resistance equals to $\frac{1}{R_{eq}} = \frac{2}{R_B}$. This implies that the flow nonuniformity is controlled by one part only which is by the barrier channels. The hydraulic resistance for circular and slit barrier channels are shown in Eqs. 18 and 19, respectively. The relation between R_B and the hydraulic diameters are to the power 4 and 3 for circular and slit geometry, respectively. Which matches well the result shown in Figure 6. Note that Eq. 19 is for infinite parallel-plate channels and only accurate for the slit geometry when $W \gg H$

$$R_{B,\text{circular}} = \frac{128\mu L}{d^4} \tag{18}$$

$$R_{B,\text{slit}} = \frac{12\mu L}{H^3\, W} \tag{19}$$

When using a low hydraulic resistance in the barrier channels, the hydraulic resistances of the manifold and reaction channels start to contribute to the flow nonuniformity. That is why $\frac{\sigma(\tilde{q}_B)}{\sigma(d_B)}$ reduces as $\Delta\tilde{P}_B$ reduces. For the same hydraulic resistance in the barrier channels and when the fabrication tolerance in the slit and circular barrier channels geometries are the same, the flow nonuniformity for the slit channel geometry is less by more than 20%. Thus, barrier channels with increasing width over depth are preferable

$$\sigma(\tilde{q}_B)_{\text{Circular}} = 4\frac{\Delta\tilde{P}_B}{1+\Delta\tilde{P}_B}\,\sigma(d_B) \tag{20}$$

$$\sigma(\tilde{q}_B)_{\text{slit}} = 2.65\frac{\Delta\tilde{P}_B}{1.56+\Delta\tilde{P}_B}\,\sigma(d_B) \tag{21}$$

To extract an empirical correlation for $\sigma(\tilde{q}_B)$ so that it can be used in the design methodology, the result in Figure 6 were fitted numerically, which are shown in Eqs. 20 and 21 for circular and slit barrier channels, respectively.

Influence of the mixers and reaction channels flow nonuniformity factor, $\sigma(\tilde{q}_C)$

The variation in the inner diameters of the mixers, reaction channels can be grouped into one parameter which is $\sigma(\Delta P_C)$. This is the variation in pressure drop over the mixers and reaction channels. By varying the inner diameter of the mixers and reaction channels, a wider range of $\sigma(\Delta P_C)$ is generated numerically. For each $\sigma(\Delta P_C)$, $\sigma(\tilde{q}_C)$ can be calculated at different $\Delta\tilde{P}_B$ as shown in Figure 7.

The mixer and reaction channels flow nonuniformity factor $\sigma(\tilde{q}_C)$ linearly increases as $\sigma(\Delta P_C)$ increases, while it inversely decreases as $\Delta\tilde{P}_B$ increases. This trend can be fitted with Eq. 22 which provides the required correlation for the mixers and reaction channels flow nonuniformity factor, $\sigma(\tilde{q}_C)$

$$\sigma(\tilde{q}_C) = \frac{\sigma(\Delta P_C)}{\Delta\tilde{P}_B} \tag{22}$$

By considering the experimental results obtained by Al-Rawashdeh et al.[21] for the influence of $\Delta\tilde{P}_B$ on the flow nonuniformity, it was possible to experimentally validate Eq. 22 as shown in Figure 8. Eq. 22 predicts the liquid flow nonuniformity with an accuracy of more than 90%. For the gas phase, Eq. 22 predicts well the flow nonuniformity but only at higher value of $\Delta\tilde{P}_B$. At lower $\Delta\tilde{P}_B$, Eq. 22 under predicts the gas flow nonuniformity. It is possible that this deviation is due to some inaccuracy in the flow and pressure drop measurements, which were for experiments performed at atmospheric conditions and lower $\Delta\tilde{P}_B$ of less than 50 mbar.

The influence of the three flow nonuniformity factors combined

The obtained correlations for $\sigma(\tilde{q}_M)$, $\sigma(\tilde{q}_B)$, and $\sigma(\tilde{q}_C)$ can be used for evaluating how much each of these factors contribute to the overall flow nonuniformity. This is done by plotting $\Delta\tilde{P}_B$ vs. the variation in the inner diameter of the barrier channels, $\sigma(d_B)$, at different conditions.

By varying $\sigma(\Delta P_C)$ from 5 to 100%, the influence of $\sigma(\tilde{q}_C)$ is analyzed as shown in Figure 9(a). As $\sigma(\Delta P_C)$ increases, $\Delta\tilde{P}_B$ needed to keep $\sigma(\tilde{q})$ less than 10% increases linearly with a ratio of almost one. Independent of $\sigma(\Delta P_C)$, there is a cut-off value for $\sigma(d_B)$ to reach a given target flow nonuniformity, which is here 10%. $\sigma(d_B)$ should not exceed this cut-off value. When $\sigma(d_B)$ is larger than the cut-off value, whatever value of $\Delta\tilde{P}_B$ is used, the target flow nonuniformity will not be obtained.

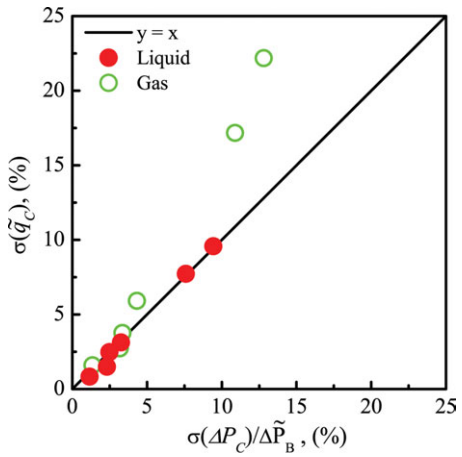

Figure 8. Experimental flow nonuniformity $\sigma(\tilde{q}_C)$ at different $\Delta\tilde{P}_B$ and $\sigma(\Delta P_C)$ taken from Al-Rawashdeh et al.[21] compared to Eq. 22.

[Color figure can be viewed in the online issue, which is available at wileyonlinelibrary.com.]

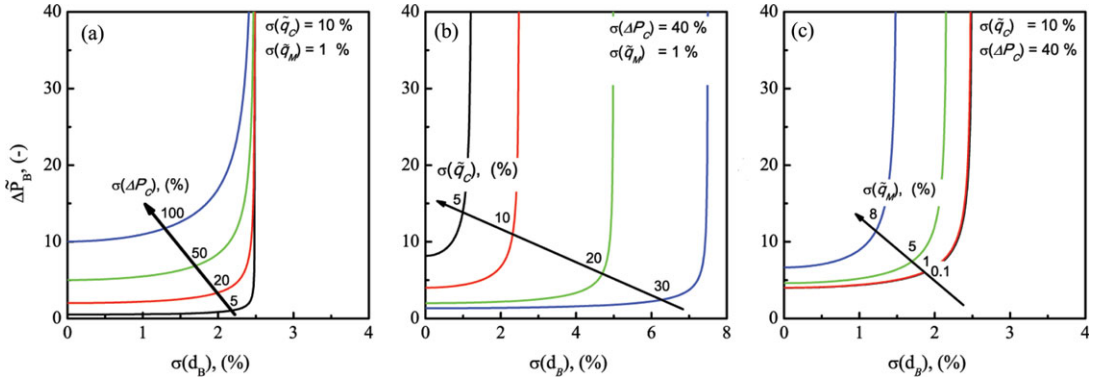

Figure 9. The influence of the three flow nonuniformity factors demonstrated by plotting $\Delta\tilde{P}_B$ versus $\sigma(d_B)$.

In (a), $\sigma(\Delta P_C)$ is varied at constant $\sigma(\tilde{q})$ of 10% and $\sigma(\tilde{q}_M)$ of 1%. (b) shows $\sigma(\tilde{q})$ when it changes at constant $\sigma(\Delta P_C)$ of 40% and $\sigma(\tilde{q}_M)$ of 1%. In (c), $\sigma(\tilde{q}_M)$ is varied at constant $\sigma(\tilde{q})$ of 10% and $\sigma(\Delta P_C)$ of 40%. [Color figure can be viewed in the online issue, which is available at wileyonlinelibrary.com.]

By varying $\sigma(\tilde{q})$, the influence of the barrier channels flow nonuniformity factor, $\sigma(\tilde{q}_B)$ is analyzed as shown in Figure 9b. When allowing a larger nonuniformity of the target flow, a lower $\Delta\tilde{P}_B$ is required and the maximum allowed variation in the barrier diameters $\sigma(d_B)$ increases. As $\sigma(\tilde{q})$ increases from 5 to 30%, the maximum allowed $\sigma(d_B)$ increases from 1 to 7%. This demonstrates the trade off between flow nonuniformity and the fabrication tolerance.

The influence of flow nonuniformity factor due to the manifold is shown in Figure 9c. As $\sigma(\tilde{q}_M)$ increases to 5% [half that of $\sigma(\tilde{q})$] its influence on $\Delta\tilde{P}_B$ and $\sigma(d_B)$ remains almost the same. When it increases to 8%, which is 80% of $\sigma(\tilde{q})$, the maximum allowed $\sigma(d_B)$ reduces and $\Delta\tilde{P}_B$ increases. It can be conclude that when $\sigma(\tilde{q}_M)$ is less than half of the target flow nonuniformity, then $\sigma(\tilde{q}_M)$ has little influence on $\sigma(d_B)$ and $\Delta\tilde{P}_B$.

Correlation of $\sigma(\Delta P_C)$ for Taylor flow regime

An important finding of this work is Eq. 22, in specific $\sigma(\Delta P_C)$. This parameter contains, the variation in the diameter of the mixer and reaction channels, the flow regime, physical properties, and the multi-phase flow nonuniformity. It represents the scaling-parameter for the process of numbering-up. From a design point of view, this parameter provides the maximum allowed variation in the channel diameters of the mixer and reaction channels. Therefore, a direct correlation to link $\sigma(\Delta P_C)$ to the variation in the inner diameters is required. Obtaining such a correlation for gas-liquid Taylor flow is demonstrated.

Using the 2-PRN model, the variation in the inner diameter of the mixer and reaction channels is shown in Figure 10. A 10% maximum variation in the channels diameter is generated numerically following Eq. 14 as presented in the design methodology. The variation in the diameter of the mixer channels is implemented for the mixer channels depth H_{mixer} and for the width of the inlet gas channel $W_{\text{mixer},G,\text{in}}$. At each variation, $\sigma(\Delta P_C)$ is calculated at different values of $\Delta\tilde{P}_B$. The result are then normalized by $\Delta\tilde{P}_B$ as shown in Figure 10

$$f_d = a\,\frac{\sigma(d)}{\Delta\tilde{P}_B} \tag{23}$$

$$\frac{\sigma(\Delta P_C)}{\Delta\tilde{P}_B} = \sigma(\tilde{q}_C) = \sqrt{(f)^2_{dC} + (f)^2_{W_{\text{mixer},G,\text{in}}} + (f)^2_{H_{\text{mixer}}}} \tag{24}$$

A linear relations are observed between $\sigma(\Delta P_C)$ and the variation in the channels diameter. By fitting the result using Eq. 23, correlations for d_C, $W_{\text{mixer},G,\text{in}}$, and H_{mixer} can be obtained. The values of the constant (a) for the three correlations and their 95% confidence intervals are shown in Table 4. By combing the correlations for d_C, $W_{\text{mixer},G,\text{in}}$ and H_{mixer}, one can predict $\frac{\sigma(\Delta P_C)}{\Delta\tilde{P}_B}$ as shown in Eq. 24.

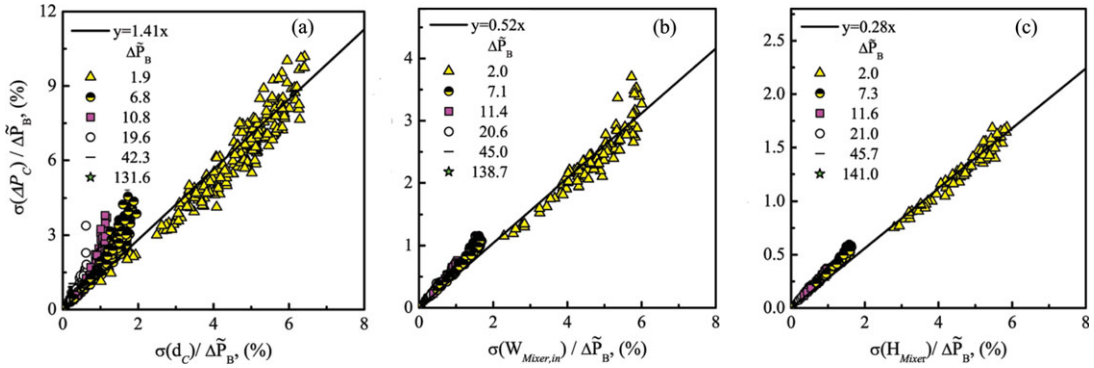

Figure 10. Influence of the variation in the inner diameter of the mixer and reaction channels on $\frac{\sigma(\Delta P_C)}{\Delta\tilde{P}_B}$ at different value of $\Delta\tilde{P}_B$.

(a)–(c) shows the result of the variation in $\sigma(d_C)$, $\sigma(W_{\text{Mixer},G,\text{in}})$ and $\sigma(H_{\text{Mixer,in}})$ all normalized by $\Delta\tilde{P}_B$, respectively. [Color figure can be viewed in the online issue, which is available at wileyonlinelibrary.com.]

Table 4. Values of the Fitting Parameter and their 95% Confidence Intervals for Different Equations

	a	95% confidence intervals
$f_{d_C} = a\ \frac{\sigma(d_C)}{\Delta\tilde{P}_B}$	1.41	1.40–1.42
$f_{W_{mixer,G,in}} = a\ \frac{\sigma(W_{mixer,G,in})}{\Delta\tilde{P}_B}$	0.52	0.52–0.53
$f_{H_{mixer}} = \frac{\sigma(\delta_{H_{mixer}})}{\Delta\tilde{P}_B}$	0.28	0.27–0.29

Assessing the role of fabrication tolerance on $\sigma(\Delta P_C)$, is a major contribution of this design methodology. Depending on the application, it is possible that fouling or deposition of material occur over time. In such a scenario what should be done is anticipating the level of fouling in advanced. The influence of fouling on the variation in the pressure drop, $\sigma(\Delta P_C)$ should be determined or estimated. In this way, $\sigma(\Delta P_C)$ takes into account not only the fabrication tolerance but also the influence of fouling or deposits. This will result in a new requirement for the barrier channels. Thus, $\sigma(\Delta P_C)$ is a generic parameters which takes into account all the effects in the mixer and reaction channels.

Design methodology

The design methodology is summarized in Figure 11. In the first step, the given input is specified: physical properties, mixer and reaction channels dimensions, and target flow nonuniformity. Based on the fabrication process technology, in the second step, the maximum acceptable variation in the inner diameter for the barrier, mixer and reaction channels is specified. Next, the hydraulic resistances which can be considered zero are specified. The fourth step is to find the manifold dimensions. By specifying the percentage of the manifold flow nonuniformity of the target flow nonuniformity, Eq. 16 or the 2-PRN model can be used to estimate the manifold hydraulic resistance R_M. This provides an estimate for the manifold dimensions. The fifth step is to calculate the remaining flow nonuniformity factors. Depending on the barrier channel geometries (slit or circular), Eq. 20 is used to calculate the barrier channels flow nonuniformity factor. Using Eq. 6, the mixer and reaction channel flow nonuniformity factor are calculated. The sixth and last step is to calculate the barrier channel dimensions. The 2-PRN model or Eq. 22 are used to calculate $\Delta\tilde{P}_B$, which can be directly used to calculate the needed $\Delta\overline{P}_B$ and the barrier channels dimensions.

As there is a trade off between the fabrication tolerance and the barrier channels dimensions, the design methodology may require iteration to reach a realistic design. In Appendix, the design methodology is demonstrated using a numerical example.

Conclusion

This article presents a design methodology for a multiphase barrier-based flow distributor. It is based on the 2-PRN model which is applied to different microchannels dimensions and geometries. The model quantitatively demonstrates the effects of fabrication tolerances on the flow nonuniformity. It shows that:

- For the same fabrication tolerance, barrier channels with slit geometry have a 20% better flow uniformity than those with a circular geometry.
- For a given target flow nonuniformity, there is a cut-off value for the allowed variation in the diameter of barrier channels $\sigma(d_B)$. $\sigma(d_B)$ should not exceed this cut-off value. For example, for a flow nonuniformity of less than 10%, the cut-off value of $\sigma(d_B)$ is 2.5 and 3.5% for circular and slit barrier channels geometries, respectively.
- When the flow nonuniformity due to the manifold $\sigma(\tilde{q}_M)$ is less than 50% of the target flow nonuniformity, reducing $\sigma(\tilde{q}_M)$ does not affect the maximum allowed $\sigma(d_B)$ or the needed $\Delta\tilde{P}_B$.

A key outcome of the design methodology is the correlation for $\sigma(\Delta P_C)$. The variation in the pressure drop over the mixers and reaction channels. This parameter contains, the variation in the diameter of the mixer and reaction channels, flow regime, physical properties, and multi-phase flow nonuniformity. Thus, it can be regarded as a scaling parameter for numbering-up. If a pressure drop correlation is available for a new flow regime or multiphase flows, the current design methodology can easily be modified by adjusting the correlation of $\sigma(\Delta P_C)$.

It is important to note that the hydraulic RN used in this design methodology is only valid for relatively low *Re* number in the laminar regime. However, for larger *Re* numbers, the hydraulic flow resistances due to flow turning, contraction, expansion, and mixing (singularity losses) can not be neglected and strongly influence the manifold performance. This is an issue of flow distribution for single phase flow which can be approached separately. For the influence of the

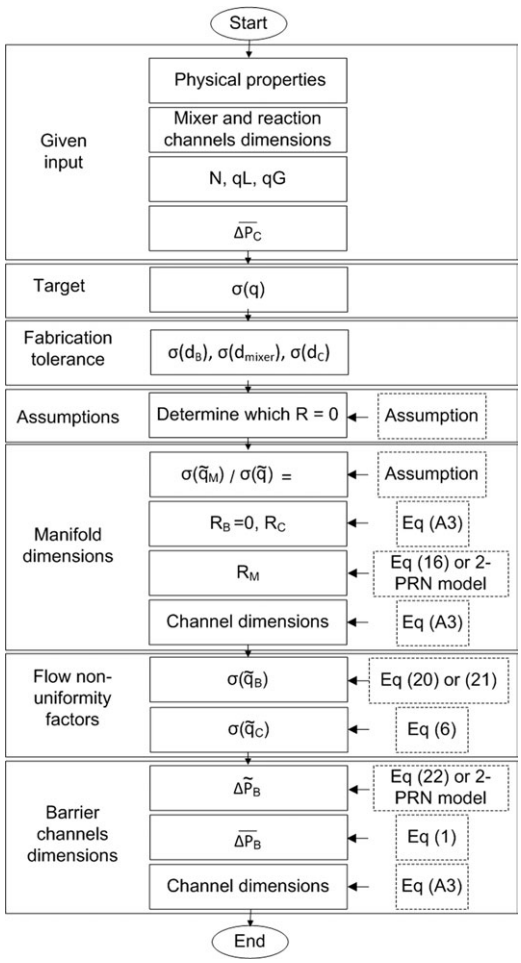

Figure 11. Step-by-step design methodology for barrier-based multiphase flow distributor.

variation in the inner diameter of the barrier channels, no changes are anticipated at larger *Re* numbers. For the influence of mixer and reaction channels factor, which is the essence of this work, a case study using a detailed fluid mechanics analysis (numerical and/or experimental) can only bring clear answers to this question.

Acknowledgments

The authors gratefully acknowledge the financial support by the Dutch Technology Foundation (STW) project number (07979) with the support from the Industrial Advisory Board (IROP) of the Netherlands Research School in Process Technology (OSTP) and Micronit.

Notation

A = channel cross-section area, m^2
A_b = bubble cross-section area, m^2
Ca_b = capillary number based on the liquid properties and the gas bubble velocity
Ca_{gl} = capillary number based on the liquid properties and sum of the superficial gas and liquid velocities
d = channel nominal hydraulic diameter, m
H = channel height, m
H_{mixer} = depth of T-mixer channels, m
L = channel length, m
W = channel width, m
$W_{mixer,G,in}$ = width of inlet gas channel in a T-mixer, m
N = number of channels
P = pressure, Pa
q = flow rate, m^3
R = hydraulic resistance, $\frac{Pa\,s}{m^3}$
Re = Reynolds number
Re_{GL} = Reynolds number of the liquid based on the sum of the superficial gas and liquid velocities
L = channel length, m
U = superficial velocity, m/s′

Greek letters

δ_s = correction on slug length to account for the nose and tail of bubble, m
δ_f = random tolerance added to the inner diameter of a channel to simulate the fabrication tolerance, m
λ_{NC} = non-circularity factor depends on the channel geometry
μ = viscosity Pa.s
ρ = density, kg/m^3
ζ_c = singularity loss due to sudden contraction
ζ_e = singularity loss due to sudden increase in cross section area
ζ_m = singularity loss due to combining two branches
ζ_s = singularity loss due to splitting of two branches
ζ_t = singularity loss due to turning

subscript

M = manifold channel
B = barrier channel
C = gas–liquid flow channel
S = separator channel
E = exit channel
T = t-mixer
G = gas
L = liquid

Literature Cited

1. Mills PL, Quiram DJ, Ryley JF. Microreactor technology and process miniaturization for catalytic reactions-A perspective on recent developments and emerging technologies. *Chem Eng Sci*. 2007;62: 6992–7010.
2. Mason BP, Price KE, Steinbacher JL, Bogdan AR, McQuade DT. Greener approaches to organic synthesis using microreactor technology. *Chem Rev*. 2007;107:2300–2318.
3. Hartman RL, Jensen KF. Microchemical systems for continuous-flow synthesis. *Lab Chip*. 2009;9:2495–2507.
4. Hessel V. Novel process windows - gate to maximizing process intensification via flow chemistry. *Chem Eng Technol*. 2009;32: 1655–1681.
5. Hessel V, Cortese B, de Croon M. Novel process windows - concept, proposition and evaluation methodology, and intensified superheated processing. *Chem Eng Sci*. 2011;66:1426–1448.
6. Kockmann N, Gottsponer M, Roberge DM. Scale-up concept of single-channel microreactors from process development to industrial production. *Chem Eng J*. 2011;167;718–726
7. Shao N, Gavriilidis A, Angeli P. Flow regimes for adiabatic gas-liquid flow in microchannels. *Chem Eng Sci*. 2009;64:2749–2761.
8. Rebrov EV, Ekatpure RP, de Croon MHJM, Schouten JC. Design of a thickwalled screen for flow equalization in microstructured reactors. *J Micromech Microeng*. 2007;17:633–641.
9. Rebrov EV, Ismagilov IZ, Ekatpure RP, de Croon MH, Schouten JC. Header design for flow equalization in microstructured reactors. *AIChE J*. 2007;53:28–38.
10. Hessel V, Knobloch C, Löwe H. Review on patents in microreactor and micro process engineering. *Recent Patents Chem Eng*. 2008;1:1–16.
11. Schenk R, Hessel V, Hofmann C, Löwe H, Schönfeld F. Novel liquid-flow splitting unit specifically made for numbering-up of liquid/liquid chemical microprocessing. *Chem Eng Technol*. 2003;26:1271–1280.
12. Losey M, Schmidt M, Jensen K. Microfabricated multiphase packed-bed reactors: characterization of mass transfer and reactions. *Ind Eng Chem Res*. 2001;40:2555–2562.
13. de Mas N, Gunther A, Kraus T, Schmidt M, Jensen K. Scaled-out multilayer gas-liquid microreactor with integrated velocimetry sensors. *Ind Eng Chem Res*. 2005;44:8997–9013.
14. Wada Y, Schmidt M, Jensen K. Flow distribution and ozonolysis in gas-liquid multichannel microreactors. *Ind Eng Chem Res*. 2006;45:8036–8042.
15. Angeli P, Gavriilidis A. Hydrodynamics of Taylor flow in small channels: a review. *Proc IME C J Mech Eng Sci*. 2008;222:737–751.
16. Kreutzer MT, Gunther A, Jensen KF. Sample dispersion for segmented flow in microchannels with rectangular cross section. *Anal Chem*. 2008;80:1558–1567.
17. He Q, Hasegawa Y, Kasagi N. Heat transfer modelling of gas-liquid slug flow without phase change in a micro tube. *Int J Heat Fluid Flow*. 2010;31:126–136.
18. Gupta R, Fletcher DF, Haynes BS. CFD modelling of flow and heat transfer in the Taylor flow regime. *Chem Eng Sci*. 2009;65:2094–2107.
19. Fries DM, von Rohr PR. Liquid mixing in gas-liquid two-phase flow by meandering microchannels. *Chem Eng Sci*. 2009;64:1326–1335.
20. Kececi S, Wörner M, Onea A, Soyhan HS. Recirculation time and liquid slug mass transfer in co-current upward and downward Taylor flow. Presented at 3rd International Conference on Structured Catalysts and Reactors, ICOSCAR-3, Ischia, Italy, 27–30 September 2009.
21. Al-Rawashdeh M, Fluitsma L, Nijhuis T, Rebrov E, Hessel V, Schouten J. Design criteria for a barrier-based gas-liquid flow distributor for parallel microchannels. *Chem Eng J*. 2012; 181–182; 549–556.
22. Amador C, Gavriilidis A, Angeli P. Flow distribution in different microreactor scale-out geometries and the effect of manufacturing tolerances and channel blockage. *Chem Eng J*. 2004;101:379–390.
23. Commenge JM, Falk L, Corriou JP, Matlosz M. Optimal design for flow uniformity in microchannel reactors. *AIChE J*. 2002;48:345–358.
24. Warnier M, de Croon M, Rebrov E, Schouten J. Pressure drop of gas-liquid Taylor flow in round micro-capillaries for low to intermediate Reynolds numbers. *Microfluidics Nanofluidics*. 2010;8:33–45.
25. van Steijn V, Kleijn CR, Kreutzer MT. Predictive model for the size of bubbles and droplets created in microfluidic T-junctions. *Lab Chip*. 2010;10:2513–2518.
26. Rebrov EV, Schouten JC, de Croon MH. Single-phase fluid flow distribution and heat transfer in microstructured reactors. *Chem Eng Sci*. 2010;66:1374–1393.
27. Pan M, Tang Y, Yu H, Chen H. Modeling of velocity distribution among microchannels with triangle manifolds. *AIChE J*. 2009;55: 1969–1982.

Appendix

2-PRN model

The 2-PRN model is used to compute the the flow distribution in parallel channels by solving the pressure drop equations and the mass balances for both gas and liquid

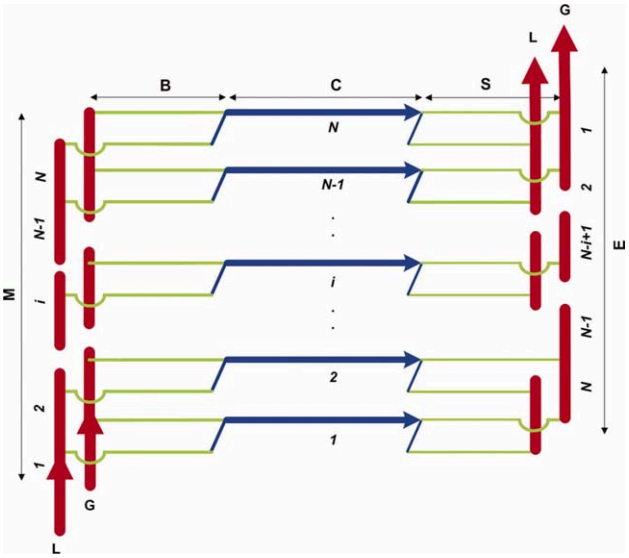

Figure A1. Schematic view for gas–liquid flow in multiple parallel microchannels.

Variables mentioned are: (M) manifold, (B) barrier channels, (C) reaction channels, (S) gas–liquid separator channels, (E) Exit or collector channels, (N) number of channels, (G) gas, and (L) liquid. [Color figure can be viewed in the online issue, which is available at wileyonlinelibrary. com.]

simultaneously. An extended 2-PRN for gas–liquid flow is shown in Figure A1.

Pressure drops balance. For any consecutive loops, such as the one shown in Figure A2, there are two possible flow paths between one junction in the manifold to one junction in the exit. The pressure drop of the two flow baths are equal. For each flow path, the pressure drop is a summation of the pressure drops of the flow segments as shown in Eqs. A1 and A2 for the gas and liquid, respectively. For each phase, an $(N - 1)$ equations are obtained.

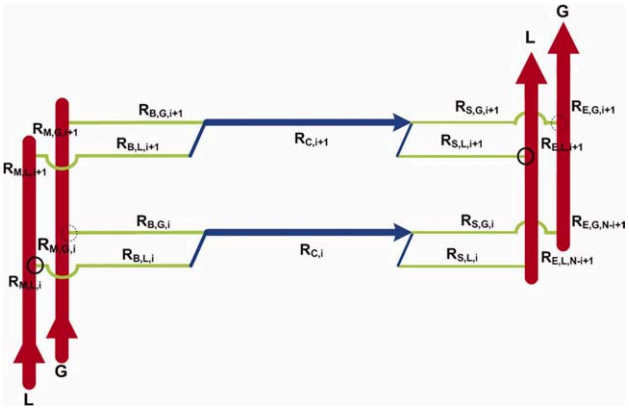

Figure A2. Schematic view for the pressure drop balance for one loop (loop rule) for 2 reaction channels.

The pressure drop balance for liquid and gas is made between the complete and dotted circle, respectively. [Color figure can be viewed in the online issue, which is available at wileyonlinelibrary.com.]

$$\Delta P_{B,L,i} + \Delta P_{C,i} + \Delta P_{S,L,i} + \Delta P_{E,L,(N-i+1)} - (\Delta P_{M,L,i+1} + \Delta P_{B,L,i+1} + \Delta P_{C,i+1} + \Delta P_{S,L,i+1}) = 0, \quad \text{(A1)}$$

$$\Delta P_{B,G,i} + \Delta P_{C,i} + \Delta P_{S,G,i} + \Delta P_{E,G,(N-i+1)} - (\Delta P_{M,G,i+1} + \Delta P_{B,G,i+1} + \Delta P_{C,i+1} + \Delta P_{S,G,i+1}) = 0, \quad \text{(A2)}$$

$i = 1,2,\ldots\ldots, (N - 1)$.

The pressure drop in Eqs. A1 and A2 can be written in hydraulic resistance format as $\Delta P = R\ q$. For each ΔP_i, the hydraulic resistance R is a summation of different types of hydraulic resistances as shown in Table A1.

R_{friction} is the hydraulic resistance due to the frictional losses caused by the wall shear in the channel. For laminar flow in channels, the Hagen–Poiseuille equation can be used to estimate the pressure drop for a given flow rate q.[23] Thus, R_{friction} can be written as shown in Eq. (A3), where μ is the viscosity, L is the channel length, λ_{NC} is a non-circularity factor that depends on channel geometry,[22] A is the channel cross section area, and d is the hydraulic diameter.

$$R_{\text{friction}} = \frac{32\mu L\lambda_{NC}}{d^2 A} \quad \text{(A3)}$$

$R_{\text{singularity}}$ is the hydraulic resistance due to the losses caused by splitting the flow into two branches, sudden contraction in the cross section area and stream turning losses. For the inlet singularity losses, $R_{\text{singularity,inlet}}$, it is computed according to Eq. A4; where as for the exit singularity $R_{\text{singularity,outlet}}$, it is computed according to Eq. A5.

$$R_{\text{singularity, inlet}} = (\zeta_s + \zeta_C + \zeta_t)\frac{\rho}{2A}U \quad \text{(A4)}$$

$$R_{\text{singularity, outlet}} = (\zeta_m + \zeta_e + \zeta_t)\frac{\rho}{2A}U \quad \text{(A5)}$$

ζ_s, ζ_c, ζ_t, ζ_m, and ζ_e are the singularity losses factors due to splitting of two branches, sudden contraction, turning, combining two branches, and sudden increase in cross section area, respectively.[27]

R_{mixing} is the hydraulic resistance caused by mixing the gas and liquid, computed according to Eq. A6.

$$R_{\text{mixing}} = (\zeta_m)\frac{\rho}{2A}(U_G + U_L) \quad \text{(A6)}$$

$R_{\text{multiphase}}$ is the hydraulic resistance for the multiphase flow in the reaction channel. In our case, $R_{\text{multiphase}}$ corresponds to the gas–liquid Taylor flow resistance which is caused by the wall shear in the channel, the capillary force and the slug sizes as shown in Eqs. A7–A9.[24] Re_{GL} and Ca_{GL} are the Reynolds and capillary numbers for the gas–liquid flow, A_b is the gas bubble cross section area, and δ_s is the length of the cap in the liquid slug.

Table A1. Types of Hydraulic Resistances in the Flow Network Shown in Figure A1 and their Summation to Compute ΔP_i

Flow rate	Resistance	R_{friction}	$R_{\text{singularity}}$	R_{mixing}	$R_{\text{multiphase}}$
$q_{M,i+1}$	$R_{M,i+1} =$	$(R_{i+1}$	$+ R_{\text{inlet},i+1})$		
q_i	$R_{B,i} =$	(R_i)			
q_i	$R_{C,i} =$	(R_i)			
$q_{G,i} + q_{L,i}$	$R_{C,i} =$			$(R_i$	$+ R_i)$
q_i	$R_{S,i} =$	(R_i)			
$q_{E,(N-i+1)}$	$R_{E,(N-i+1)} = (R_{,(N-i+1)} + R_{\text{outlet},(N-i+1)})$				

$$R_{\text{multiphase}} = \frac{2\mu L \lambda_{NC}}{d^2 A}\,(Re_L\, f_s) \tag{A7}$$

$$f_s = \frac{16}{Re_{GL}}\left(1 + a\frac{d_C}{L_s + \delta_s}\left(\frac{Re_{GL}}{Ca_{GL}}\right)^{0.33}\right) \tag{A8}$$

$$a = \frac{7.163^{\frac{2}{3}}}{32}\left(\frac{A}{A_b}\right)\left(\frac{Re_{GL}}{Ca_{GL}}\right)^{\frac{1}{3}}\left(Ca_b^2 + 3.34Ca_b\right)^{-1} \tag{A9}$$

Note that $R_{\text{singularity}}$, R_{mixing}, and $R_{\text{multiphase}}$ are flow rate dependent. As they are used to calculate the flow rate, a numerical iteration will be required in the solving procedure.

Mass balance. By applying mass balance at each junction (junction rule), the flow rates in the manifold distributor, $q_{M,(i+1)}$, and exit collector, $q_{E,(N-i+1)}$, are expressed as a function of the flow rates in the parallel channels. They are presented in Eqs. A10 and A11, respectively.

$$q_{M,(i+1)} = \sum_{k=1}^{k=N} q_k - \sum_{k=1}^{k=i} q_k \tag{A10}$$

$$q_{E,(N-i+1)} = \sum_{k=1}^{k=i} q_k \tag{A11}$$

The total gas and liquid inlet flow rates can be written as in Eqs. A12 and A13, respectively.

$$q_{G,\text{inlet}} = \sum_{k=1}^{k=N} q_{G,k} \tag{A12}$$

$$q_{L,\text{inlet}} = \sum_{k=1}^{k=N} q_{L,k} \tag{A13}$$

Solver. By rearranging the mass balances and the pressure drop balances, a set of algebraic equations is generated as shown below. The $M_{\text{resistances}}$ is a systematic matrix which includes all the hydraulic resistances. As the $M_{\text{resistances}}$ is quite large to show, Table A2 shows an example of the $M_{\text{resistances}}$ for $N = 4$.

Table A2. An Example for the Resistance Matrix $M_{\text{resistances}}$ Performed when $N = 4$

$(R_{B,L,1}+R_{C,1}+R_{S,L,1}+R_{E,L,4}+R_{M,L,2})$	$R_{C,1}$	$-(R_{B,L,2}+R_{C,2}+R_{S,L,2})$	$-R_{C,2}$	0		0		0		0		
$R_{C,1}$	$(R_{B,G,1}+R_{C,1}+R_{S,G,1}+R_{E,G,4}+R_{M,G,2})$	$-R_{C,2}$	$-(R_{B,G,2}+R_{C,2}+R_{S,G,2})$	0		0		0		0		
$(R_{E,L,3}+R_{M,L,3})$	0	$(R_{B,L,2}+R_{C,2}+R_{S,L,2}+R_{E,L,3}+R_{M,L,3})$	$R_{C,2}$	$-(R_{B,L,3}+R_{C,3}+R_{S,L,2})$	$-R_{C,3}$			0		0		
0	$(R_{E,G,3}+R_{A,G,3})$	$R_{C,2}$	$(R_{B,G,2}+R_{C,2}+R_{S,G,3}+R_{E,G,3}+R_{M,G,3})$	$-R_{C,3}$	$-(R_{B,G,3}+R_{C,3}+R_{S,G,2})$			0		$-(R_{B,L,4}+R_{C,4}+R_{S,L,1})$	$-R_{C,4}$	
$(R_{E,L,2}+R_{M,L,4})$	0	$(R_{E,L,2}+R_{M,L,4})$	0	$(R_{B,L,3}+R_{C,3}+R_{S,L,2}+R_{E,L,2}+R_{M,L,4})$	$R_{C,3}$	$(R_{B,G,3}+R_{C,3}+R_{S,G,2}+R_{E,G,2}+R_{M,G,4})$		$-R_{C,4}$		$-(R_{B,G,4}+R_{C,4}+R_{S,G,1})$		
0	$(R_{E,G,2}+R_{M,G,4})$	0	$(R_{E,G,2}+R_{M,G,4})$	$R_{C,3}$		0		1		0		
1	0	1	0	1		1		0		1		
0	1	0	1	0		0		1		0		

TA2

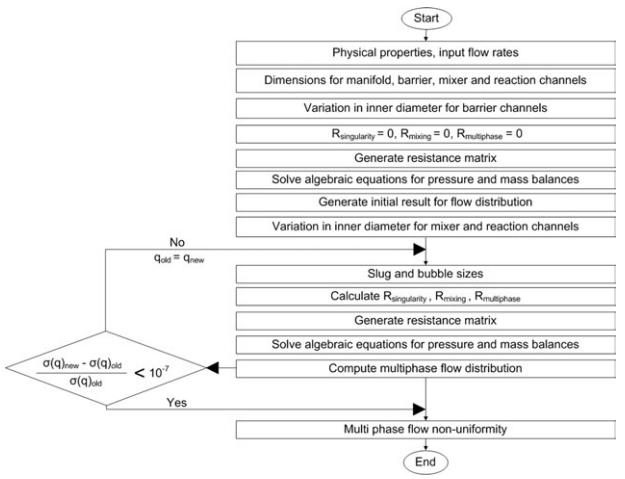

Figure A3. Sequence procedure for solving the 2-PRN model.

$$M_{\text{resitances}} \times \begin{pmatrix} q_{\text{L},1} \\ q_{\text{G},1} \\ \vdots \\ q_{\text{L},i} \\ q_{\text{G},i} \\ \vdots \\ q_{\text{L},N-1} \\ q_{\text{G},N-1} \\ q_{\text{L},N} \\ q_{\text{G},N} \end{pmatrix} = \begin{pmatrix} R_{\text{M,L},2} \times q_{\text{L,in}} \\ R_{\text{M,G},2} \times q_{\text{G,in}} \\ \vdots \\ R_{\text{M,L},i} \times q_{\text{L,in}} \\ R_{\text{M,G},i} \times q_{G,\text{in}} \\ \vdots \\ R_{\text{M,L},N} \times q_{\text{L,in}} \\ R_{\text{M,G},N} \times q_{\text{G,in}} \\ q_{\text{L,in}} \\ q_{\text{G,in}} \end{pmatrix}$$

The procedure to generate the $M_{\text{resistances}}$ and solve the algebraic equations is presented in Figure A3. Matlab 7.5.0 is used to perform the calculations. Once the model generates the results, the manifold, barrier, mixer, and reaction channels dimensions can be tuned to reach the desired design.

Manuscript received Oct. 8, 2011, and revision received Jan. 3, 2012.